

# Adjustable Aerobraking Heat Shield for Satellites Deployment and Recovery

S. Pagano, R. Savino

**Abstract** — The paper deals with a minisatellite equipped with a variable geometry aerobraking thermal protection device. Satellites with deployable heat shield can be easily accommodated in folded configuration in the fairing of the launch vehicle upper stage. When deployed before reentry, they increase the surface area and therefore the aerodynamic drag, to achieve larger deceleration at high altitudes, where the atmosphere is more rarefied. This may be important in order to reduce heat fluxes, pressures and thermomechanical loads to survive re-entry. In particular, the proposed system has the ability to adjust the opening degree of the heat shield, deploying and retracting the drag device during the guidance and navigation phase, so that the satellite is able to accomplish a controlled de-orbiting phase to re-enter the atmosphere at a desired location. During the final hot re-entry phase, the shield is completely deployed with the maximum exposed surface area so that the satellite re-entry module is able to survive the temperatures and mechanical stresses reaching without damages the target point on Earth.

**Keywords** — Artificial satellite, thermal protection system, deployable system, articulated linkage.

## I. INTRODUCTION

Some scientific or exploration space missions, for instance biology or physical sciences in microgravity, require to safely recover the payload or the flight data on Earth. Actually ensuring payload recovery is difficult and expensive. Larger space systems generally have dedicated thrusters to execute a precise de-orbit burn initiating the re-entry trajectory. Because deorbit generally occurs within one or two orbits after the de-orbit burn, the re-entry guidance can be computed on the ground and uplinked to the spacecraft, leaving the spacecraft navigation and control system responsible only for tracking the precomputed guidance. Due to high heat fluxes and aerodynamic loads in the atmospheric re-entry phase complex and expensive thermal protection systems (TPS), made of ablative or heavy ceramic materials, are employed. In recent years, the miniaturization of technology has brought about small spacecraft that may not contain thrusters or attitude control systems, and generally do not perform active re-entry control. These satellites have generally been built by

universities and small organizations as teaching tools or testbeds for low-cost scientific experiments or technology demonstrations. As such, benign materials are generally used, and most components of the spacecraft are destroyed during re-entry and pose no threat to ground assets. However, there is currently an increasing demand for small satellites capable of performing reentry missions. In this case a reliable de-orbiting system is necessary with the requirements of low cost, low mass and volume, high resistance to thermo-structural loads in the phases of atmospheric re-entry and aerodynamic heating.

Thermal protection systems with aerobraking functions are also known as *para-shield*, because they have the double function of aerodynamic drag devices (*parachute*) and of *heat shield*. The para-shield concept and its features were discussed by Akin in 1990 [1]; the large surface exposed to the air flow allows to obtain a low ballistic coefficient and thus to reduce dynamic pressure and thermal loads to values compatible with the use of off-the-shelf materials such as glass-based or ceramic-based fabrics and materials.

Deployable heat shields offer the advantage of decoupling the ballistic coefficient from the volumetric requirements of the launcher, allowing to optimize the aerodynamic characteristics in the re-entry phase. Therefore, the satellite has high ballistic coefficient when the heat shield is folded, similar to those of traditional capsules or spacecrafts in the launch phase, characterized by ballistic coefficients in the order of 250-1000 kg/m<sup>2</sup>. It becomes lower than 50 kg/m<sup>2</sup> when the shield is deployed, ensuring a suitable aerodynamic drag to decelerate the capsule in the re-entry phase. In any case, if the final landing/splashing speed is greater than that required for a soft impact on ground (depending on the requirements of the mission) a parachute can be adopted.

In order to recover the payload contained in the satellites re-entry modules, in the past two decades, different variable geometry TPS have been developed, all characterized by small overall dimensions before launch. In [2], an inflatable TPS is presented while in [3, 4] a deployable system is proposed. In particular, concepts of deployable re-entry systems have been suggested at the University of Naples Federico II, in collaboration with small medium and large Italian enterprises [5,6,7]. Due to the shape and to the principle of operation, these deployable systems are called *umbrella like TPS*. They are constituted by slats, hinged to the re-entry module, sustaining a fabric sheet resistant to high temperatures.

This paper proposes a satellite with a re-entry module, containing the recoverable payload, equipped with an

---

Manuscript received March 06, 2017; revised March 16, 2017.

S. Pagano is with the *Dipartimento di Ingegneria Industriale, Università degli Studi di Napoli Federico II*, 80125 ITALY, (e-mail: pagano@unina.it).

R. Savino is with the *Dipartimento di Ingegneria Industriale, Università degli Studi di Napoli Federico II*, 80125 ITALY, (e-mail: rasavino@unina.it).

umbrella like deployable TPS. It allows to control the de-orbiting phase of the re-entry module and therefore the trajectory and the landing/splashing target point on the Earth, with sufficient accuracy (maximum error of about 10 km). The TPS consists of a ceramic-based fabric, supported by articulated slats, driven by an electric actuator, which allows to vary the TPS deployment degree and therefore the ballistic coefficient of the re-entry module. It is so possible to adjust the satellite speed and the thermo-mechanical loads acting on the shield.

## II. SATELLITE DESCRIPTION

The proposed satellite [8] includes a service module and a re-entry module:

- the re-entry module (Fig.1), with its payload bay, is equipped with an *umbrella-like* mechanism to deploy and modulate the heat shield, having also the function of aerobrake. The re-entry module also includes a rigid hemispherical nose and other subsystems needed for the mission, e.g. the ceramic fabrics for the conical deployable aero-brake, lightweight, temperature-resistant material (e.g. carbon fiber composites) for the hemispherical nose, linear actuators, batteries, sensors, recovery systems. The *nose* and the *conical aeroshell* fabrics are supported by several articulated slats;
- the service module includes on-board data handling (OBDH), power, telecommunication, attitude control systems, thermal control systems. The external surface is coated with solar cells.

The two modules are connected (Fig.2) until the satellite reaches a relatively low altitude so that the atmosphere density is high enough. After the separation of the two modules, due to severe aero-heating conditions, corresponding to the most critical leg of the atmospheric hypersonic re-entry trajectory, the service module completely destroys and burns while the re-entry module, thanks to the presence of the deployed heat shield, gently decelerates, survives heat and mechanical loads approaching safely the Earth.

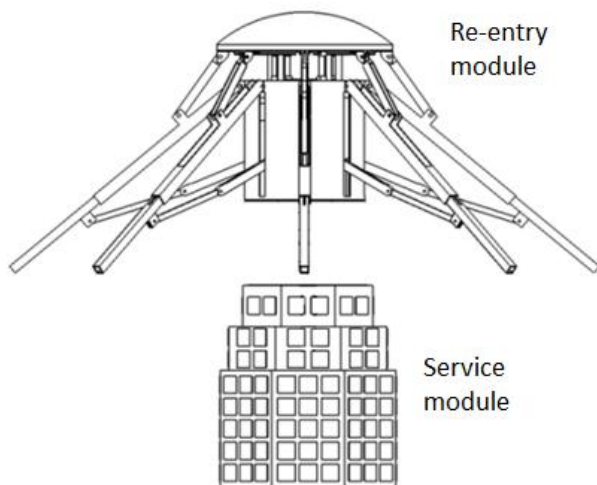


Fig. 1. The two modules of the satellite

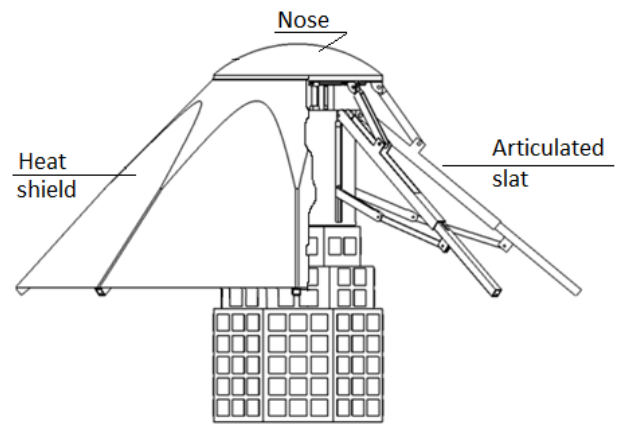


Fig. 2. Satellite with deployed heat shield

In particular, the re-entry module consists of:

- a cylindrical payload bay;
- a nosecone, placed in the forward part of the capsule, including the nose, a base connection plate and an inner thermal insulator;
- a deployable umbrella-like heat shield, able to thermally protect the container during the atmospheric re-entry.

The modulation of the heat shield, acting as a deceleration drag device before the critical atmospheric entry phase, is fundamental to control the de-orbiting phase and re-enter the atmosphere at a desired location, depending on the target impact point on the Earth. The heat shield is made of ceramic fabric and has a tronco-conical shape; its smallest base is fixed to the nosecone while the largest one is fixed to the end of the slats. The fabric itself may be an off-the-shelf material, such as 3M™ -Nextel™ [9] made of metal oxide fibers (alumina  $Al_2O_3$ , Boron oxide  $B_2O_3$ , silica  $SiO_2$ ) that is typically used as thermal protection in many industrial and aerospace applications in presence of flames or other high temperature sources. The fibers of the Nextel fabric have a melting temperature of about 2000 °C.

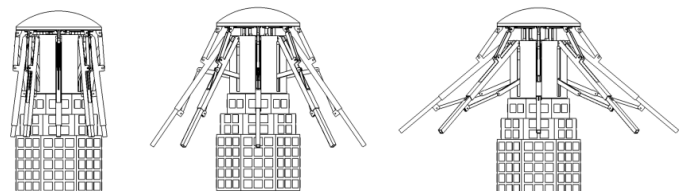


Fig. 3. Deployment sequence

According to previous studies [5, 6, 7], for a module with a recovery mass of about 20kg, the following requirements apply to the heat shield:

- when fully deployed, the total exposed surface area should be about 1 m<sup>2</sup>; an aeroshell fabric with 45° angle with respect to the module axis is aerodynamically stable;
- in the folded configuration, the shield fabrics must not cover the solar cells arranged on the underlying surface of the service module; for this reason, the slats supporting the fabric have to be retracted in the folded configuration. The slats must then elongate during the

deployment phase to increase the surface area exposed to the airflow, according to the deployment sequence represented in Fig. 3, where the fabric is not shown. To this end, particular articulated slats have been considered.

### III. SHIELD DEPLOYMENT MECHANISM

The shield is deployed by means of a particular extendable articulated mechanism, schematically represented in Fig. 4. It is a planar closed-chain mechanism (each member has more than one coupling) constituted by three ternary members (frame, nose and rocker arm) and four binary members (extern link, internal link, push rod, extender).

Considering the container as the frame of the mechanism, the other mobile members are connected by means of eight revolute pairs and two prismatic pairs; the mechanism mobility is therefore equal to one. The input parameter, that can be independently controlled, is the prismatic pair variable connecting the nose displacement with respect to the frame..

The deployment of the slats is driven by linear actuators, not shown in the figure, set in the container and acting on the nose.

With reference to the kinematic scheme (Fig.5), the frame is represented by the fixed points  $A, B$  and by the linear guide  $g_1$ .

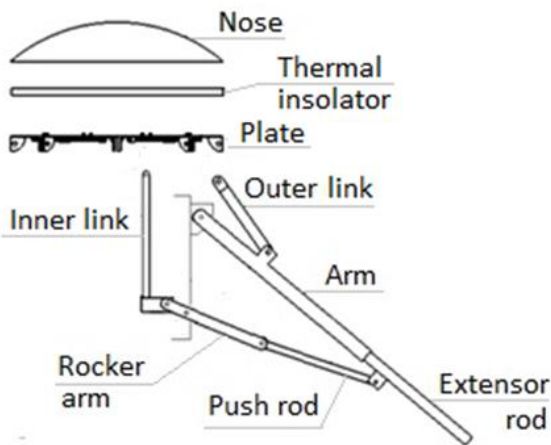


Fig. 4 -Articulated slat

The nose drives the following two links:

- the *outer link* connecting the nose to the arm that is hinged on the container so that, the nose displacement causes the arm rotation with respect to the capsule axis.
- the *inner link*, connecting the nose to the *rocker arm* that is pivoted in the fixed point  $B$ . The rocker arm inverts and amplifies the inner link motion and acts on the *push rod* that push the *extender rod* from the arm engaging the linear guide  $g_2$ .

By means of a snap type mechanical lock, it is possible to fix the position of the extensor, with respect to the arm, when the mechanism reaches the maximum degree of deployment.

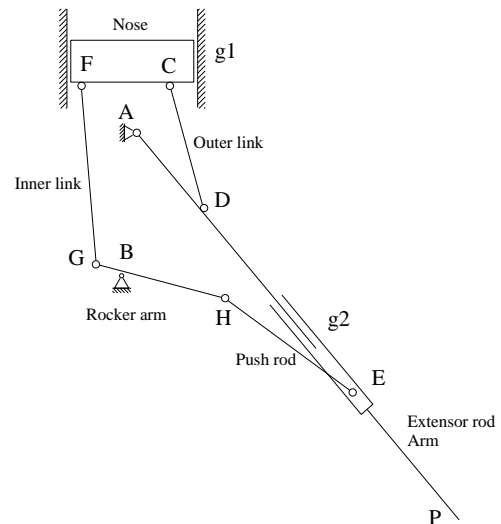


Fig. 5 - Scheme of the slat mechanism

The mechanism has the following advantages:

- all the slats are deployed adopting only one linear actuator or with more linear actuators acting in parallel and placed between the container and nose;
- the shield fabric is deployed and tensed, moving away the nose, that is hottest part of the module, from the container;
- only the extreme parts of the extenders are in contact with the hot fabric. For these parts it is necessary the adoption of particular temperature-resistant material (e.g. ceramic materials). The other parts are not in direct contact with hot fabric and therefore are exposed to a relatively low temperature allowing the use of ordinary materials, however, resistant to high temperatures (metal or ceramic machinable);
- in the folded configuration, the fabric does not cover the solar cells placed on the outer surface of the service module.

Figure 6 shows the trajectory described by extreme point of the extensor (point  $P$ ) during the deployment phase. The figure shows also the circular trajectories that point  $P$  would describe considering the extender locked in fully retracted position ( $R_i$  radius) and in fully extended position ( $R_o$  radius,).

The figure shows that it is possible to detect a nose position for which the elongation of the slat is maximum ( $R_o$  radius); a further displacement of the nose from the container would imply a reduction of the slat length as the extender would move in the opposite direction with respect to the arm.

In the present case, the maximum slat elongation is equal to about the 40% of the retracted slat length, with an arm rotation of about  $46^\circ$ , with respect to the module axis, and a nose displacement of about 26 mm.

Fig. 7 represents the arm rotation and the slat length versus the nose displacement; the markers on the two curves indicate the mechanism configuration for which the maximum elongation of the slats is reached.

The shield deployment occurs at high altitudes, where the air resistance and the gravitational force are negligible; actions contrasting the shield deployment are therefore the tension of the fabric sheet and the friction forces acting in the mechanism

joints.

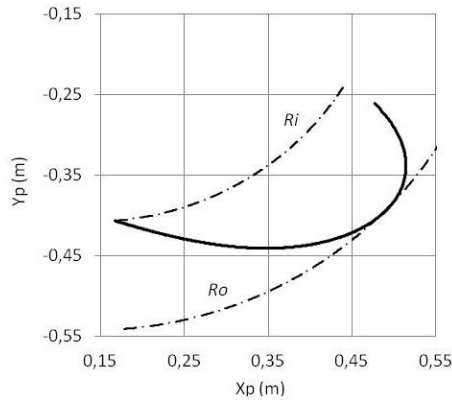


Fig. 6 – Slat extremity trajectory

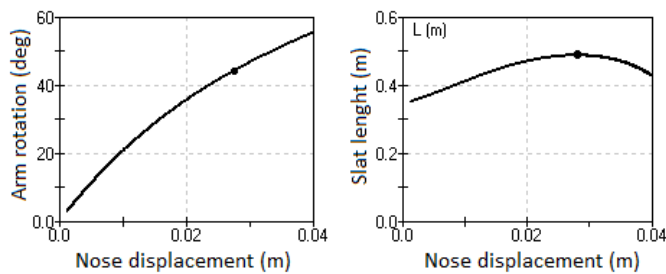


Fig. 7 – Arm rotation and slat length vs nose displacement

During the initial phase of the deployment (Fig. 8a), the nose pulls the outer and the inner links and therefore:

- the outer link exerts the force  $F_8$  on the arm. This force produces a moment, with respect to the hinge (A), which induces the rotation of the arm;
- the inner link exerts the force  $F_{11}$  on the rocker arm lifting its inner end. The outer end moves in opposite direction and its amplitude is about 4 times greater. Therefore, the force acting on the outer end of the rocker arm is roughly equal to  $F_{11}/4$ ; its component, acting along the push rod axis direction ( $F_{13}$ ) pushes the extender out of the arm. In the initial part of the deployment, force  $F_{13}$  has two components having different effect: the component  $F_{13,a}$  pulls the extender from the arm while the moment caused by  $F_{13,p}$  (orthogonal to the arm axis) with respect to point A, tends to fold the slat.

It can be observed that force  $F_{13,p}$  has a magnitude that is smaller than  $F_8$  magnitude but it has a greater distance from hinge A. For greater arm angles,  $F_{13,p}$  rapidly reduces in magnitude and the resulting moment tends to rotate the arm outwards.

It follows that there is an angular position of the arm from which the positive moment (clockwise), generated by the outer link, is certainly greater than the negative one, which originates from the action of the inner link. The arm therefore must not reach too small angles otherwise it may not unfold. This circumstance is however avoided as the diameter of the service modulus is larger than the container diameter (Fig. 2) preventing small angles of the arm with respect to the axis of the module.

To achieve the maximum deployment of the shield it would be necessary that point H (connection between the rocker arm and the push rod) exceeds the line joining points B and E (Fig. 9).

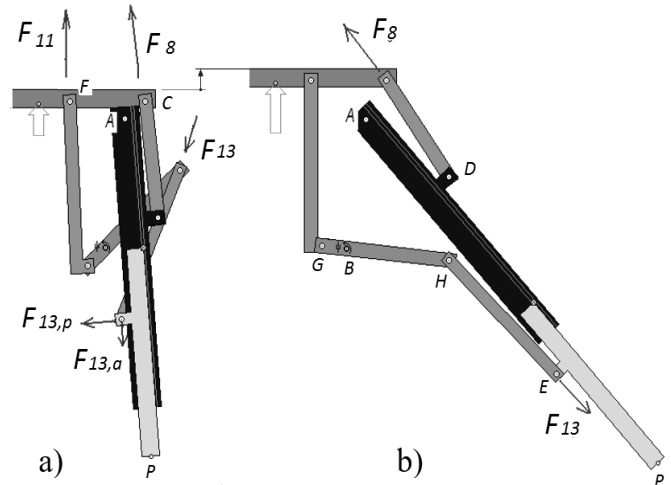


Fig. 8 – Forces acting on the slat

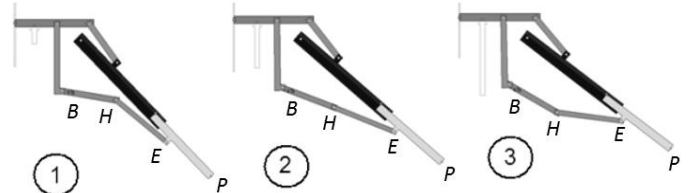


Fig. 9 – Relative angular position between the rocker arm and the push rod in the end phase of deployment

In the re-entry phase, the force acting on the extensor, due to the pressure on the shield, pushes the extensor itself inside the arm. The same force also has a component that tends to rotate the arm outside of the module.

By means of a latch device, the extensor is locked with respect to the arm, in the maximum deployment position so that the pressure force is contrasted by:

- the element constituted by the arm and the push rod, subjected to a tensile stress;
- the external link, that is subject to a compression stress.

#### IV. SHIELD STRESS ANALYSIS

Before the beginning of the re-entry phase, the shield is fully deployed and the fabric shield is tensioned; during the re-entry phase, the fabric tension is also due to the dynamic pressure of the airflow.

The stress analysis of the heat-shield components presents the difficulty of modelling the fabric by means of elements able to react only to tensile stresses and that its strength vary with its orientation. The problem should be solved adopting a non-linear FEM code. However, in first approximation, it is possible to use a simpler scheme, considering that the major tensile stresses arise along the fabric generatrices, passing through the extremities of the slats.

The displacement of the nose determines the slats divarication that is counteracted by the presence of the shield fabric that exerts a resistant action, along the lines joining the slats tips.

Therefore, it can be assumed that the fabric absorbs the tensioning forces mainly along the following lines:

- the generatrices of the truncated cone-shaped shield, passing through the slat tips;
- the segments joining through the tips of consecutive slats, along the shield edge.

The corresponding forces are absorbed by fictitious fabric tapes disposed along the above-mentioned directions (Fig. 9). Using a FEM code is possible to model the tapes and all the components constituting the slats, taking into account their actual configuration. In this way, it is also possible to check individual components against buckling.

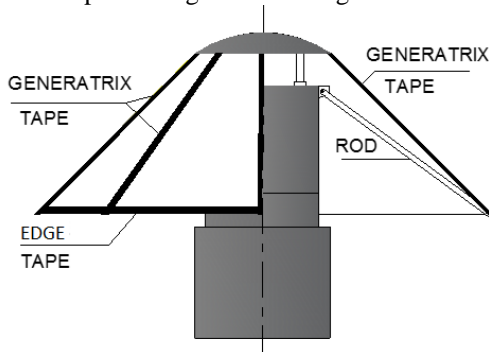


Fig. 10 – Shield tapes scheme

For the sizing of the curtain only, in a first approximation it is possible to schematize each slat with a simple bar hinged to the container, as shown in Fig.10. In this way, it is possible to solve the shield structure with a linear FEM model (Fig. 11) in which the tapes and the slats are modelled by means of bar elements reacting to axial stress.

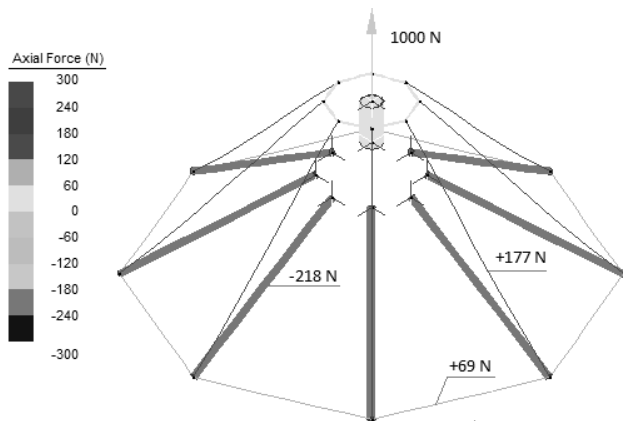


Fig. 11 – Simplified shield model. The tensile axial forces in the tapes and the compression axial forces in the bars (slats) are due to a load of 1000N acting on the nose.

The dynamic pressure acting on the shield can be introduced by appropriately increasing, the load exerted by the actuators on the nose. This simple model allows to estimate the axial stress in the tapes or the actuator force necessary to appropriately tension the fabric (the tapes). This model assumes particular significance if the fabric shield is reinforced with tapes, made of the same fabric material, superimposed to the shield, and arranged in correspondence of the sheet generatrix and along the sheet edge, thus realizing a

light shield, reinforced along the directions where the stresses are higher.

## V. DYNAMIC PRESSURE ON THE SHIELD

An approximate evaluation of the pressure acting on the shield can be derived by assuming that the re-entry module falls on Earth following a vertical direction and that the re-entry module have constant attitude. The aerodynamic supersonic drag coefficient is assumed equal to 1. The motion of the re-entry module is then described by the following equation:

$$\frac{1}{2} \rho v^2 C_D S = mg + m \frac{dv}{dt}$$

(1)

or, equivalently:

$$\frac{1}{2} \frac{\rho}{B} v^2 = g + \frac{dv}{dt}$$

(2)

being:

- $m$ , the re-entry module mass;
- $\rho$ , the air density;
- $C_D$ , the drag coefficient;
- $S$ , reference area, equal to the projected frontal area of the heat shield;
- $v$ , the flow velocity relative to the module;
- $g$ , the gravitational acceleration.

The term:

$$B = \frac{m}{C_D S}, \quad (3)$$

is the *ballistic coefficient*, that describes how the air resistance slows the body motion.

In equation (2), it must be taken into account that the air density,  $\rho$ , of and the gravitational acceleration,  $g$ , vary with the altitude. In particular, the variation of the air density, with the altitude  $h$ , depends on pressure and on temperature, both decreasing with altitude and having opposite effects. The air density is evaluated with the following expressions [10]:

- o for  $h < 11$  km:  $\rho = \rho_0 [1 - (6.5/288) * h]^4.255$ ;
- o for  $h > 11$  km:  $\rho = \rho_{11} * e^{-0.1575 * (h-11)}$ ;

being:  $\rho_0$  and  $\rho_{11}$  the air density at the sea level (1,225 kg/m<sup>3</sup>) and at the altitude of 11 km (evaluated with the first expression);  $h$  is the altitude in kilometers.

Indicating with  $R_T$  the Earth radius ( $R_T = 6.38 \cdot 10^6$  m), the gravitational acceleration variation versus altitude is:

$$g = g_0 \frac{R_T^2}{(R_T + h)^2} \quad (5)$$

Eq. 4 and 5 are plotted in Fig. 12.

A simulation of the re-entry module motion was carried out assuming the following parameters: re-entry module mass,  $m = 20$  kg; drag coefficient,  $C_D = 1$ ; frontal projection area of the shield,  $S = 1$  m<sup>2</sup>. The ballistic coefficient is therefore:  $B = 20$

$\text{kg/m}^2$ , much smaller than the value that it assumes when the shield is folded (about  $280 \text{ kg/m}^2$ ).

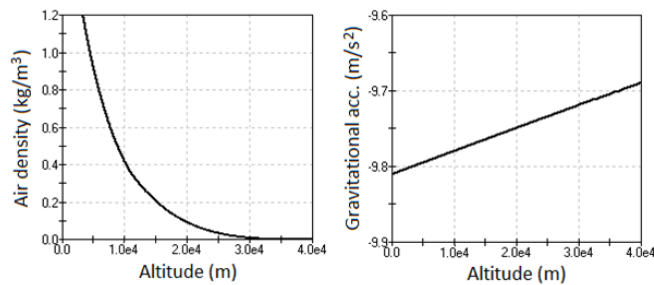


Fig. 12. Air density and gravitational acceleration vs altitude

The simulation was conducted considering null initial velocity at the altitude of 300 km. It can be observed that:

- the re-entry module acceleration is quite constant, until the maximum velocity of about 2100 m/s is reached as, in this phase, the aerodynamic force assumes low values and the weight is quite constant. Then, the module decelerates in a marked way at the altitude of about 60 km (Fig. 13);

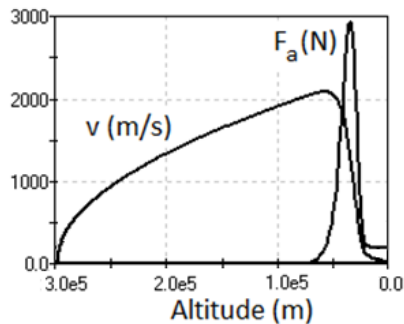


Fig. 13. Aerodynamic force and velocity vs altitude

- the sea level is reached after about 1020 s (17 min);
- the final velocity is about:  $v_f = 20 \text{ m/s}$ ;
- the maximum deceleration occurs at the altitude of about 40 km;
- the aerodynamic force achieves its maximum (2840 N) at the altitude of about 42 km;
- in such conditions the maximum pressure acting on the shield is equal to 2.8 kPa;
- the pressure force is very small if the altitude is greater than about 75 km; above this altitude, it is therefore possible to adjust the shield degree of deployment with lower power consumption as the only force that opposes the deployment of the shield is that due to the fabric tensioning, that is important only in the final part of the deployment.

Fig. 14 and 15 report the velocity and the acceleration of the re-entry module for two different initial values altitude: 300 km and 90 km.

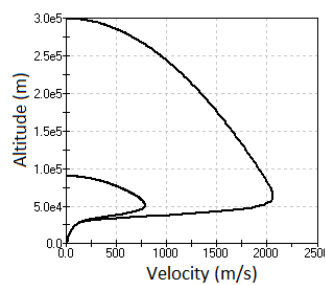


Fig. 14. Altitude-velocity diagram

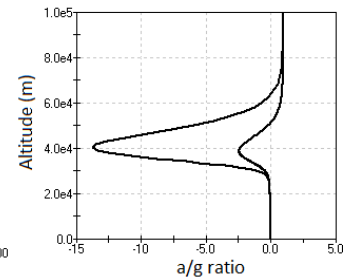


Fig. 15. Altitude-a/g diagram

## VI. CONCLUSIONS

The paper presents a minisatellite characterized by a heat shield with adjustable airbrake function to control the de-orbiting phase and to re-enter the atmosphere at a desired location. The shield is sustained by a particular mechanism characterized by extendable slats. Mechanism kinematic analysis shows that in the folded configuration, it does not cover the solar cells arranged on the service module.

To overcome the difficulties of the stress analysis of the shield fabric, related to elements not resistant to compressive stresses, a simple approximate criterion is presented.

## REFERENCES

- [1] Akin, D.L. - The parachield entry vehicle concept: basic theory and flight-test developments. 4th Annual AIAA/Utah State University Conference on Small Satellites, Logan, UT, 1990.
- [2] Andrews, J., Watry, K., Brown, K.: Nanosat de-orbit and recovery system to enable new missions. 25th Annual AIAA/USU Conference on Small Satellites, Logan, UT, 2011.
- [3] R. Savino, V. Carandente, Aerothermodynamic and feasibility study of a deployable aerobraking re-entry capsule, Fluid Dynamics and Material Processing 8(4) pp. 453-477 (2012)
- [4] Wiegand M., Königsman H.J. - A Small Re-entry Capsule BREMSAT2 - 10th AIAA/USU Small Satellite Conference, Logan, UT, 1996.
- [5] Savino R., Aurigemma R., Carandente V., Gramiccia L., Longo J., Marraffa L., Funzo F., "Study and Development of a Sub-Orbital Reentry Demonstrator" *J. British Interplanetary Society*, Vol. 62, n. 2, 74-81 (2014).
- [6] Iacovazzo M., Savino R., Zuppari G., Carandente V. Longitudinal stability analysis of a suborbital re-entry demonstrator for a deployable capsule", *Acta Astronautica*, Volume 106, January-February 2015, 101-110 (2015)
- [7] Carandente V., Savino R., D'Oriano V., Fortezza R., "A Study on Earth Re-entry Capsules with Deployable Aerobrakes for Recoverable Microgravity Experiments" *Microgravity Science and Technology*, Volume 27, June 2015, 181-191 (2015)
- [8] Pagano S., Savino R.. - Satellite con aerofreno e protezione termica dispiegabile in modo controllato. Patent request number 102016000016905 - 18.2.2016
- [9] 3M Nextel: [http://solutions.3mdeutschland.de/3MContentRetrievalAPI/BlobServlet?lmd=1270717655000&locale=de\\_DE&assetType=MMM\\_Image&assetId=1258565166920&blobAttribute=ImageFile](http://solutions.3mdeutschland.de/3MContentRetrievalAPI/BlobServlet?lmd=1270717655000&locale=de_DE&assetType=MMM_Image&assetId=1258565166920&blobAttribute=ImageFile)
- [10] J.D. Anderson - Introduction to flight - McGraw Hill Book Company, 1989.